ADDITIONAL QUADRUPOLES AT CENTER OF LONG STRAIGHTS IN THE NSLS-II LATTICE *

F.Lin#, J.Bengtsson, W.Guo, S.Krinsky, Y.Li, L.Yang, BNL, NY, 11973 USA

Abstract

The NSLS-II storage ring lattice is comprised of 30 DBA cells arranged in 15 superperiods. There are 15 long straight sections (9.3m) for injection, RF and insertion devices and 15 shorter straights (6.6m) for insertion devices. In the baseline lattice, the short straights have small horizontal and vertical beta functions but the long straights have large horizontal beta function optimized for injection. In this paper, we explore the possibility of installing additional quadrupoles at the center of selected long straight sections in order to provide two low-beta source locations for undulators in the same straight. The required modification to the linear lattice is discussed as well as the preservation of adequate dynamic aperture required for good injection efficiency and adequate Touschek lifetime.

INTRODUCTION

The NSLS-II baseline storage ring lattice has 9.3m long straight sections to accommodate injection, RF cavities and DWs and other user IDs. Large horizontal beta function in the long straights is employed for reducing the betatron amplitude during the top-off beam injection. However, the high- β_x function increases the photon beam size and impairs the brightness of insertion devices. In another PAC'11 paper [1], we describe how we can successfully reduce the horizontal beta function in a symmetric set of long straights by changing the strength of the existing quadrupoles in the baseline lattice. This modified lattice can still preserve an adequate dynamic aperture for good injection efficiency and adequate Touschek lifetime. In this paper, we will present an additional scheme to reduce the horizontal beta function by installing additional quadrupoles at the center of the long straight. This method can produce two low-beta sources for each long straight.

Lattice modification starts from the lattice with high-low β_x function in the long straights obtained in paper [1]. We retain the fixed positions of the baseline lattice: injection point at the 30th cell, three damping wigglers (DW) at the 8th, 18th and 28th cell for a 3-fold symmetry, and RFs are at the 22nd (and 24th cell for more insertion devices), a 3-fold symmetric ring layout is presented in Figure 1, where LSH represents long straight with high β_x function, LSL represents long straight with low β_x function (no additional quadrupoles at the center) and LS2L represents long straight with two low β_x function source locations. In this type of allocation, the injection point at LSH can maintain large horizontal beta function for the top-off injection. Meanwhile the low β_x function in the LSL optimizes the brightness of damping wigglers and insertion devices and low β_x functions in the LS2L provide increased brightness of two short insertion devices.

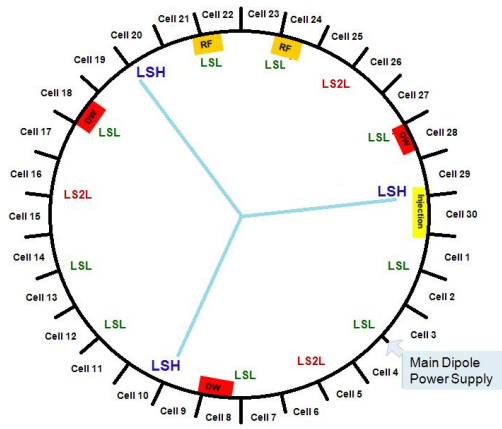

Figure 1: The modified storage ring layout with 3-fold symmetry. LSH: long straight with high β_x function, LSL: long straight with low β_x function, LS2L: long straight with two low β_x function source locations.

LINEAR OPTICS OPTIMIZATION

The linear lattice modification follows the guidelines that were applied for the original design [2, 3]: ~2nm-rad natural emittance without damping wigglers and 3 pole wigglers, horizontal chromaticity ~105 in magnitude (<6.9 per supercell i.e. 2 DBAs), β_x ~3 m and β_y ~1 m at the center of the short straight sections. Symmetry conditions are maintained at the center of the straights and at the center of the arcs. The DBA is achromatic so that the linear dispersion is zero in all of the straight sections. The maximum dispersion is at the center of the arc and is ~0.46 m which facilitates chromaticity correction with reasonable sextupole strength. More constraints are applied at the center of the insertion device: α_y =0 to ensure the symmetry of the vertical beta function at the center of insertion devices, β_x ~1.5m for an optimum vertical gap of a ~3m long insertion device, small β_x as much as possible for brightness.

A schematic drawing of the 9.3m long straight configuration with additional quadrupoles at the center is plotted in Figure 2. Two QIDFs and one QIDD comprise an quadrupole triplet symmetrically arranged at the center. Considering a reasonable 2~3 m long space occupied by these additional quadrupoles and the distance between them, the whole drift space left for insertion devices is about 7m, with each 3.5m long. Hence, approximately L~1.8m is the distance between the center of insertion device and the adjacent facilities. The length of QIDF and QIDD are chosen to be 0.3 and 0.5 respectively by

*Work supported by U.S. DOE contract No. DE-AC02-98CH10886
#flin@bnl.gov

considering a reasonable balance between the occupied space and the practical strength limit of quadrupoles.

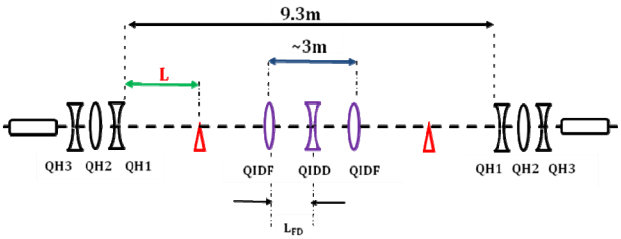

Figure 2: schematic drawing of the 9.3m long straight configuration with an quadruople triplet (2QIDF + 1 QIDD) at the center. QHs are the existing quadrupoles in the baseline lattice. The locations of triangular mark the positions of the centers of insertion devices.

We have 6 free knobs for adjusting the significant change of the local beta functions: the strengths of QIDF and QIDD, the distance L_{FD} between QIDF and QIDD, and three local QH quadrupole families bounding this long straight. To control the tunes to some specific working points, the other quadrupole families QLs bounding the short straights and QMs in the arcs between the dipole magnets are adjusted. In this study, corresponding to four different types of long straights: LSH, LSL, LS2L, LSL (DW), there are four types QH families: QHs, QHNEWs, QHIDNEWs, and QHDWs, and each family have 3 types of individuals. Plus QMs, QLs, QIDFs and QIDD, there are totally 19 quadrupole families for the linear lattice optimization.

Following the ring layout in Figure 1, a lattice with working points (37.16, 17.22) is obtained as shown in Figure 3 for 1/3 of the ring. The beta functions in the LSH and LS2L are enlarged in Figure 4 for a good view.

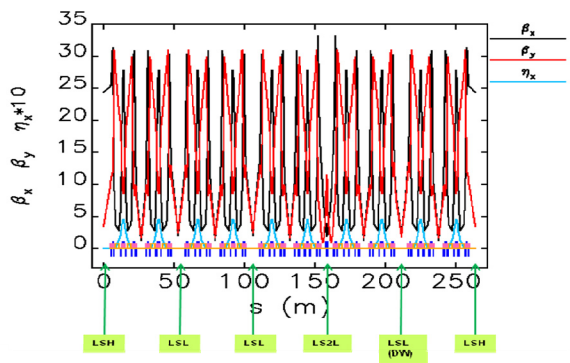

Figure 3: The lattice functions of 1/3 of the ring for working points (37.16, 17.22). (LSH: long straight with β_x, LSL: long straight with low β_x; LS2L: long straight with two low β_x sources; LSL (DW): long straight with low β_x and DW).

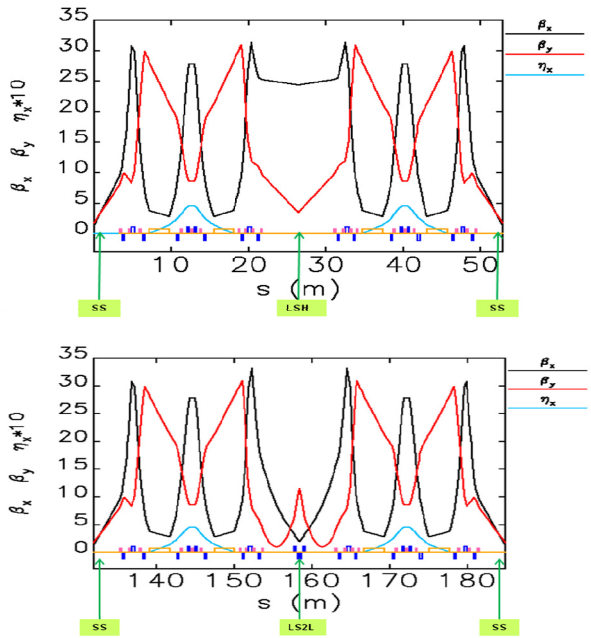

Figure 4: The lattice functions in LSH and LS2L.

NONLINEAR OPTIMIZATION

Following a similar process to optimize the nonlinear driving terms as in paper [1], moving the working point away from the leading order resonance lines is the first consideration in the linear lattice optimization. Meanwhile, to avoid the sextupoles becoming too strong, the linear lattice should be designed with horizontal chromaticity < 110 in magnitudes for the whole ring and with peak dispersion ~0.46m [2].

9 sextupoles families in each DBA cell of the NSLS-II baseline lattice are available for the nonlinear optimization in the baseline lattice. Among them 3 sextupoles families are located in the non-zero dispersion region. Two of them are determined to correct the first-order chromaticity and the remaining one, together with the other 6 sextupoles located in the zero-dispersion region, are used to compensate the second-order chromaticity, tune shift with amplitude and nonlinear resonance driving terms.

For the lattice given in Figure 3 composed of high and different types of low horizontal beta long straights and DWs, we break up some of sextupole families from the baseline lattice to introduce additional variables. Finally there are 27 sextupoles families available for the nonlinear optimization. Among them 6 of them are used for the first-order chromaticity correction and 21 for the correction of high-order chromaticity, tune shift with amplitude and resonance driving terms.

Elegant [3] is used as the simulation platform for the nonlinear optimization used in this paper. Tuning the sextupole families, analytical expressions [4, 5] of the driving terms of resonances are calculated, and the penalty function is calculated as a weighted sum of linear and nonlinear chromaticity, resonance and tune shift with

amplitude related terms. The dynamic aperture is optimized by using this approach.

Magnet misalignment errors [6] and physical apertures are considered for the calculation of dynamic aperture. Instead of modelling relatively large errors plus corrections, we can simply use random errors that result in lattice functions with errors at a corrected level. Physical apertures at NSLS-II come from the photon absorbers (±38 mm) in the horizontal plane and insertion devices in the vertical plane. For instance, the minimum vertical gap of those IDs is 5 mm of IVU U20 located at the center of short straight (SS).

Frequency maps in the (x,δ) and (x,y) space are computed by including both magnets misalignment errors and physical apertures. Figure 5 shows the tunes diffusion for particles with y=1 mm, |x|<~20 mm and momentum deviation up to ±3% in the (x,δ) space. Figure 6 shows the tune diffusion for on-momentum particles with different initial transverse postions in the (x,y) space [7]. The maps are plotted in terms of tune diffusion, which is defined as $\log_{10}^{(\Delta\upsilon_x^2+\Delta\upsilon_y^2)}/2$. Both of frequency maps in these preliminary studies show that a modest dynamic aperture can approximately reach |x| ~ 15 mm for the requirement of injection.

In this lattice, the horizontal chromaticity per supercell (2 DBA cells) changes from 6.9 to 7.5 that enlarge the strength of sextupoles in arcs for chromatic correction. This excites the first and second order driving terms for resonances and reduces the dynamic aperture. So far, the placement of quadrupoles QHs has been kept fixed in LS2L. As a refinement, the full parameter space of QHs can provide more freedom degree for chromaticity adjustment.

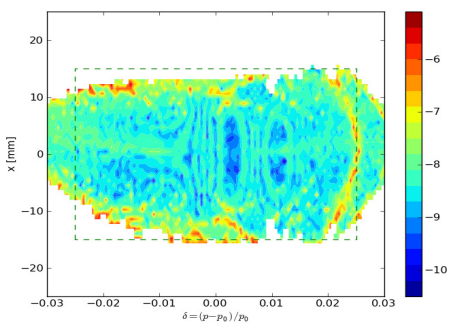

Figure 5: Frequency map in the (x, δ) space.

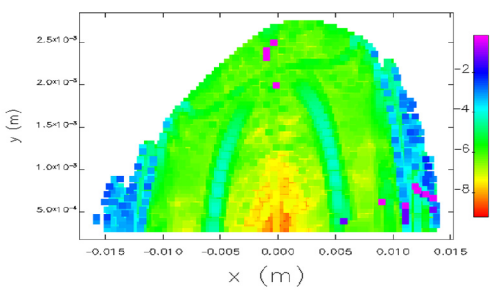

Figure 6: Frequency map in the (x, y) space.

The fractional tune footprint (ν_x, ν_y) for the same particles in frequency map Figure 5 is plotted in Figure 7. All particles are stable and have survived after 2048 turns.

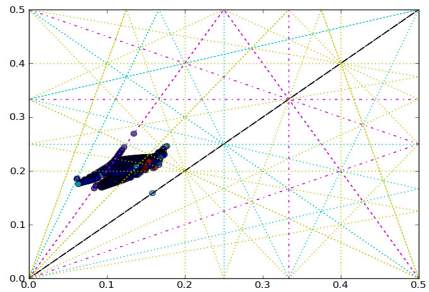

Figure 7: The fractional tunes footprint (ν_x,ν_y).

CONCLUSION

This paper discusses the possibility of producing two low-beta source locations for optimum brightness of undulators in the long straights of NSLS-II lattice by installing additional quadrupoles at the center. The linear optics is optimized to satisfy the requirements of lattice function and properties. Nonlinear optimization for a lattice with working point at (37.16, 17.22) is performed. Considering the magnets misalignment errors and physical apertures, we calculate the frequency maps and plot the tune footprint. The results show that the modified high-low beta function lattice can achieve a modest dynamic aperture in this preliminary study. Further work will continue to expand the dynamic aperture to meet the requirement of good injection efficiency and sufficient Touschek lifetime.

REFERENCE

[1] F.Lin, et.al, “Low Horizontal Beta Function in Long straights of the NSLS-II Lattice”, PAC’11.
[2] NSLS-II Preliminary Design Reports.
[3] M.Borland, http://www.aps.anl.gov/Accelerator_Systems_Division/Operations_Analysis/oagSoftware.shtml.
[4] J. Bengtsson, “The Sextupole Scheme for the Swiss Light Source(SLS): An Analytic Approach, ” SLS Note 9/97.
[5] J. Bengtsson, “NSLS-II: Control of Dynamic Aperture”, NSLS-II technical report, BNL-81770-2008-IR.
[6] W.Guo, “Re-examination of the misalignment tolerances”, NSLS-II technical report.
[7] L. Yang, “Tracking Code Development for Beam Dynamics Optimization”, PAC11.